Processing, properties and some novel applications of magnetic nanoparticles

D BAHADUR[1,*], J GIRI[1], BIBHUTI B NAYAK[1], T SRIHARSHA[1],
P PRADHAN[2], N K PRASAD[1], K C BARICK[1] and R D AMBASHTA[3]

[1]Department of Metallurgical Engineering and Materials Science; [2]School of Biosciences and Bioengineering, Indian Institute of Technology-Bombay, Mumbai 400 076, India
[3]Back-End Technology Development Division, Bhabha Atomic Research Centre, Trombay, Mumbai 400 085, India
*Corresponding author: E-mail: dhirenb@iitb.ac.in

Abstract. Magnetic nanoparticles have been prepared by various soft chemical methods including self-assembly. The bare or surface-modified particles find applications in areas such as hyperthermia treatment of cancer and magnetic field-assisted radioactive chemical separation. We present here some of the salient features of processing of nanostructured magnetic materials of different sizes and shapes, their properties and some possible applications. The materials studied included metals, metal–ceramic composites, and ferrites.

Keywords. Magnetic nanoparticles; magnetic nanocomposite; self-assembly; hyperthermia; biocompatibility.

PACS Nos 75.50; 81.07.Wx; 81.16.Dn

1. Introduction

The synthesis and functionalization of nanostructured magnetic materials has been an interesting area of study because of its possible applications in a variety of widely diversified areas ranging from information technology to nano-biotechnology. The advancements in nanofabrication and development of modern characterization techniques have opened a wide array of highly sophisticated applications of magnetic nanoparticles in the biomedical (as diagnostic and therapy) [1] as well as electronics fields [2]. The properties (physical, structural, electrical and magnetic) of magnetic nanoparticles/composites required for different applications should be unique. The coated or surface-modified (by inorganic or organic materials) and self-assembly of magnetic nanoparticles are necessary for different applications. The attachment (so-called coating) of organic molecules on the surface of particles keep them apart from each other thus providing stability, i.e., a stable suspension in liquid, called 'ferrofluid'. The inorganic coating of metal oxides or dielectric materials on the magnetic particles, i.e. core–shell structure has potential application in temperature and flow-sensors [3]. A suitable magnetic 'core–shell' nanostructure is found

to lower the 'superparamagnetic limit' due to exchange biasing [4,5]. This provides an opportunity to tailor the magnetic and electrical transport characteristics by modifying the relative dimensions of the core and the shell. The synthesis of magnetic nanoparticles through soft chemical route with different sizes and shapes is a challenging area of research [6,7]. Among the various soft chemical methods, controlled co-precipitation [8], sonochemical [9], micro-emulsion [10] and self-assembly [11] techniques have been extensively used.

Magnetic photonic crystals (MPCs) consisting of repeated dielectric elements with periods in the nano- and sub-micrometer scale regions are currently attractive due to their unique properties [12]. When the constituent material of photonic crystals is magnetic, or even if only the defect is magnetic, the resultant MPCs would exhibit very unique optical and magneto-optical properties [13,14]. The general method to fabricate 3D photonic crystals is the micromachining of a bulk material by electron beam lithography; however this approach is expensive and allows us to get only a few monolayers. The fabrication of 3D MPCs by 'self-assembly' technique is cost-effective and is also the simplest method.

The surface-modified magnetic nano or microspheres have high potential for applications involving magnetic separation of biomolecules, cell and radioactive elements. Long-lived radionuclides are to be efficiently separated in order to prevent their discharge to environment. The extractants such as crown ethers and functionalized phosphine oxides in solvated organic medium find extensive applications in the removal of radionuclides from liquid waste [15]. Loading the extractants onto resins allows lower volume requirements of the extractants for application in column-based separation method [16]. Rendering the resins magnetic enables a less complex and efficient magnetic separation methodology compared to column-based bead extraction [17]. Application of superparamagnetic substrate enables ease in filter regeneration properties. Magnetic separation method has been shown as a promising treatment process for handling fragile inorganic sorbent such as potassium nickel hexacyanoferrate (II) for the removal of cesium radionuclide [18]. Nanoaggregates of magnetite with potassium nickel hexacyanoferrate (II) improved the kinetics of the ion exchange reaction for cesium removal from aqueous medium. The distribution coefficient of coated and uncoated particles matched implying that the capacity of the sorbent is unaltered. The exchange rate of low concentration radionuclides is enhanced because nanoaggregates act as catalytic surface providing large area for reactivity. The feasibility of application of crown ether loaded magnetic microspheres for strontium removal has been demonstrated using magnetic field [19]. For the removal of lanthanides and actinides from acidic waste streams octyl(phenyl)-N,N-diisobutyl carbamoyl methyl phosphine oxides (carbamoyl methyl phosphine oxides, CMPO) find application [20]. Applicability of magnetically-assisted chemical separation studies for the removal of transuranics has been demonstrated by our studies on europium, an element following similar aqueous chemistry to americium in the acidic medium.

One of the promising applications of magnetic nanoparticles is in the hyperthermia (HT) treatment of cancer. For this, it is required to raise the temperature between 42 and 46°C for destroying the cancerous cells. Heating at higher temperatures (>56°C) causes coagulative necrosis of the tissue. In clinical hyperthermia, efforts are made to optimize thermal homogeneity of 42–46°C in the tumor tissue

by advanced therapy and thermometry system. For hyperthermia application, ferrofluids consisting of superparamagnetic as well as ferrimagnetic particles of Fe_3O_4 or γ-Fe_2O_3 have been used extensively. However, magnetic materials with Curie temperature (T_C) between 42–60°C having sufficient biocompatibility are the best candidates for effective treatment such that during therapy, they act as *in vivo* temperature control switch and thus over-heating can be avoided [21]. The systems $M_{1-x}Zn_xFe_2O_4$ (M = Mn, Co) with versatile magnetic properties have not yet been explored for hyperthermia applications [22]. Higher heating ability in the presence of AC magnetic field is determined by specific absorption rate (SAR). Higher SAR is desirable as this would require lesser dose and thereby toxicity due to overdoses may be avoided.

Biocompatibility of magnetic fluid is another important requirement for HT. Fe_3O_4 and γ-Fe_2O_3 are known to be biocompatible within certain concentration. Other substituted ferrites ($M_{1-x}Zn_xFe_2O_4$ and $Fe_{1-x}M_xFe_2O_4$, M=Co, Mn) could be superior for the same purpose. However, literature on biocompatibility of other substituted ferrites is limited. Biocompatible coating improves biocompatibility of the magnetic core and the magnetic fluid. Several surfactant and polymer-based coating materials have been tested for biocompatibility [23–25]. We have chosen fatty acid for the stabilization of magnetic particles as it is natural medium chain fatty acid and used already by pharmaceuticals and food industry. Furthermore, it gives most stable and dilution insensitive water-based magnetic fluid. Therefore, there is a need for comparative study of biocompatibility (*in vitro* and *in vivo*) of different substituted ferrites and their coated counterparts.

In this paper, we present some of our investigations on the development of magnetic nanoparticles, coated magnetic particles and their composites for potential applications like hyperthermia treatment of cancer, magnetic separation of radioactive elements and magnetic photonic crystals carried out in our laboratory in the recent past.

2. Experimental details

2.1 *Preparation of nanoparticles and their stable suspension in water*

The nanoparticles of substituted ferrites ($MnFe_2O_4$, Fe_3O_4 and $CoFe_2O_4$) and γ-Fe_2O_3 have been synthesized by soft chemical methods. These ferrite particles are modified by fatty acids and other organic media to get the water base stable suspension. The synthesis steps are discussed below.

γ-Fe_2O_3 has been synthesized by three methods. Anhydrous $FeCl_3$ was initially dissolved in ethylene glycol and KOH was added into the solution to maintain pH values. The reactions were carried out for pH values of 9, 10, 11 and 12. In the first process, the solution was kept on a hot plate at 200°C for 3 h while in the second process, the solution was refluxed for 45 min in a microwave oven. A black precipitate of γ-Fe_2O_3 settled down which was decanted with water and acetone several times [26]. The magnetic iron oxide nanoparticles have recently been synthesized by sonochemical technique where iron salt was dissolved in water and adjusted for a pH. The effect of reaction time and pH has been studied in detail.

We obtained particles of different shapes (acicular, spherical etc.) depending on the reaction conditions. The results are under investigation.

Fatty acid coated different ferrite-based magnetic fluids have been prepared by the co-precipitation technique in N_2 atmosphere. Details of the synthesis procedure are reported elsewhere [27]. In brief, stoichiometric quantities of metal chlorides were dissolved in milli Q water. Metal ion solution (0.05 M) was quickly added to the base solution (NH_4OH) with vigorous stirring and pH was adjusted to 11–12. After ageing at 95°C, the salt solution was decanted and the precipitate was repeatedly washed to remove impurity ions. This mixture containing fatty acid (30–40 wt% of ferrite) and water was heated while stirring till magnetic fluid formation. The prepared ferrofluid was purified through successive process of filtration and dialysis against de-ionized water using cellulose membrane (12.4 kDa) for 72 h. The resultant magnetic fluids were centrifuged at 5000 rpm for 10–15 min and the purified magnetic fluids were used for further characterization.

The homogeneous suspensions of nanosized γ-Fe_2O_3 particles of density 26 mg/ml and 30 mg/ml in cellulose containing distilled water have been prepared for HT applications. Initially, a homogeneous solution of cellulose was prepared in distilled water in which nanosized γ-Fe_2O_3 particles were added and stirred for one hour.

2.2 *Preparation of magnetic microsphere for magnetically-assisted radioactive waste separation*

Magnetite was synthesized in a dispersion of water–toluene in the presence of polyester dissolved in styrene monomer. The same was mixed with an aqueous dispersion of polyvinyl alcohol in the presence of benzoyl peroxide and dimethyl aniline to obtain aqueous dispersible magnetite polymer composite. The polymer surface was impregnated with the extractant CMPO $[C_8H_{17}(C_6H_5POCH_2CON(CH_2CH(CH_3)_2]$. Tracer $^{152+154}$Eu in 2N HNO_3 was studied for demonstration of transuranic radionuclide removal.

2.3 *Preparation of Ni nanoparticles and its composite materials*

Different shapes of Ni nanoparticles and Ni particles covered with NiO/ZrO_2 were synthesized by a two-stage reduction process. The first stage involves fast nucleation of the particles from an aqueous salt solution of nickel chloride and zirconium oxychloride by the reducing agent sodium borohydride ($NaBH_4$). In the second stage, these powders are heat treated in controlled atmosphere under the flow of H_2 gas at different temperatures [28]. In the case of Ni nanoparticles (with different shapes), the as-prepared powders were reduced at three different temperatures (550, 650 and 750°C) for one hour under controlled atmosphere by passing a mixture of 2% H_2 and 98% Ar. For Ni:NiO/ZrO_2 nanostructures, the as-prepared powders were reduced at 450°C for 30 min under the controlled atmosphere by passing pure H_2 gas. The by-products of reduction reaction, NaCl and H_3BO_3, remain dissolved in the aqueous solution and were removed by repeated centrifuging and washing with distilled water. The centrifuged product was dried under a lamp. Pellets were

made from the as-prepared powder and heat treated at different temperatures as mentioned above under the controlled H_2 atmosphere.

2.4 *Preparation of 3D magnetophotonic crystal*

The preparation of 3D magnetophotonic crystal involves mainly three steps. First, monodisperse spherical SiO_2 particles were prepared by hydrolysis and condensation of tetraethoxysilane (TEOS) in water–ethanol liquor in the presence of 25% NH_3 solution as a catalyst, following modified Stöber process [29]. At the beginning of the reaction, absolute ethanol, double distilled water and ammonia solution were mixed in appropriate concentration. Subsequently, TEOS was added to the above solution mixture kept under agitation by a magnetic stirrer at room temperature for two hours. In the second step, monodisperse silica spheres were coated with magnetite (Fe_3O_4) by an *in situ* reaction [30]. The reaction solution of different molar ratio of Fe^{3+}/Fe^{2+} (50 and 75%) in water was added to 10% ammoniacal solution of SiO_2 spheres for coating. For coating, SiO_2 and metal ions (Fe^{3+} and Fe^{2+}) were used in 1:1 ratio. Finally, Fe_3O_4-coated SiO_2 spheres were self-assembled into a 3D structure by applying external magnetic field.

3. Characterization

Determination of phase purity and their identification was done by X-ray diffraction (XRD) studies using Philips powder diffractometer PW3040/60 with CuK_α radiation. The crystallite size is determined from the X-ray line broadening using Scherrer formula given by

$$D = 0.9\lambda/\beta \cos \theta,$$

where D is the average crystallite size, λ is the X-ray wavelength used, β is the angular line width of half maximum intensity and θ is the Bragg's angle in degree. The infra-red spectra of the synthesized materials were obtained using a Nicolet spectrometer (Magna IR, 550). The micrographs were taken using cryo-transmission electron microscopy (Cryo-TEM) and room temperature TEM (CM 200 (Philips)) for ferrofluid and powder samples respectively. For the TEM observation, the ferrofluid sample (14–20 mg ferrite particles per ml) was diluted 10 times and then the suspension was deposited drop-wise onto a copper grid coated with carbon film and dried. The powder was first dispersed in isopropyl alcohol by ultra sonication bath (20 kHz, 500 W) and then the suspension was deposited drop-wise onto a carbon-coated copper grid and dried. The particle size was measured by the dynamic light scattering (DLS) technique, i.e. by particle size analyzer (Zeta Plus, Brookhaven Instrument). The SEM micrograph of the self-assembled Fe_3O_4-coated SiO_2 spheres was taken by ESEM (FEI Quanta – 200). The low temperature as well as room temperature magnetization was measured by VSM (Lake Shore, Model-7410). The blocking temperature (T_B) was measured based on ZFC (zero-field-cooled) and FC (field-cooled) measurements with M vs. T curve at the applied magnetic field of 200 Oe.

In vitro biological evaluation of magnetic fluids and cellulose suspended γ-ferrite was done using two cell lines BHK21 (Syrian baby hamster kidney cell line) and HeLa cell respectively, purchased from National Centre for Cell Science (NCCS), Pune, India. BHK21 cell lines were grown in basal medium eagle (BME) (Sigma-Aldrich Chemie, USA) supplemented with 10% foetal bovine serum (FBS) (Sigma-Aldrich Chemie, USA), 10% tryptose phosphate broth (Becton Dickinson, USA) and 1% antibiotic antimycotic solutions (Himedia, India). 10^4 cells (BHK 21 and HeLa) were added in each well of 96 tissue culture well plates and incubated in CO_2 incubator for 24 h. Then, ferrofluid samples were added in seven different concentrations ranging from 0.05 mg/ml to 2 mg/ml in seven different rows of 96 well plates leaving first row as control.

HeLa cells proliferation in the presence of different concentrations of cellulose suspended γ-ferrite were determined using sulforhodamine B (SRB) assay in 96 well plates as described earlier [31]. Three replicates were taken for each concentration as well as control. Then the plates were incubated for 24 h. After 24 h, sulphorhodamine B (SRB), (Sigma-Aldrich Chemie, USA) assay was done to study the cell proliferation. Percentage of viability of cells (BHK 21 and HeLa) for different concentrations was calculated as:

$$\text{Percentage viability} = \frac{\text{Absorbance of sample at 560 nm}}{\text{absorbance of control at 560 nm}} \times 100.$$

In vivo biological evaluation of magnetic fluids was done on mice models. Swiss albino mice of either sex weighing about 20–25 g within the age group of 6–8 weeks were taken for this experiment. They were provided *ad libitum* food and water. The animal experiments were approved by Institutional Animal Ethics Committee (IAEC) and all the experiments were done following the guidelines of the Committee for the purpose of control and supervision of experiments on animals (CPCSEA), India. All the mice were divided into different groups having three animals in each group.

The magnetic fluids were sterilized by autoclaving at 121°C at a pressure of 15 lb for 30 min before *in vivo* application. These were injepcted intravenously (IV) through the tail vein at three different dose rates (50 mg, 200 mg and 400 mg/kg bwt). After 1 h, 6 h and 24 h, all the animals were sacrificed under chloroform anesthesia. Blood samples were collected from heart in two different vials (one with EDTA for whole blood and other without any anticoagulant for serum) for hematological analysis. Tissue samples were collected from different organs, processed and stained with hematoxylene-eosin for morphological analysis.

4. Results and discussion

Figure 1 shows the X-ray diffraction pattern of Ni:xMZrO$_2$ nanostructures, where x corresponds to the molar concentration of Zr salt in the starting solution. Figure 2 shows the XRD patterns of SiO_2 and Fe_3O_4 coated SiO_2 particles. From figure 1 it is clear that all the structures clearly show the presence of Ni crystalline peaks. Interestingly, these lines for nickel grow in intensity with increasing ZrO_2 content. For sample at $x = 0$, the Ni particles are covered with an amorphous native oxide (NiO). With the addition of ZrO_2 the broad amorphous NiO peaks progressively
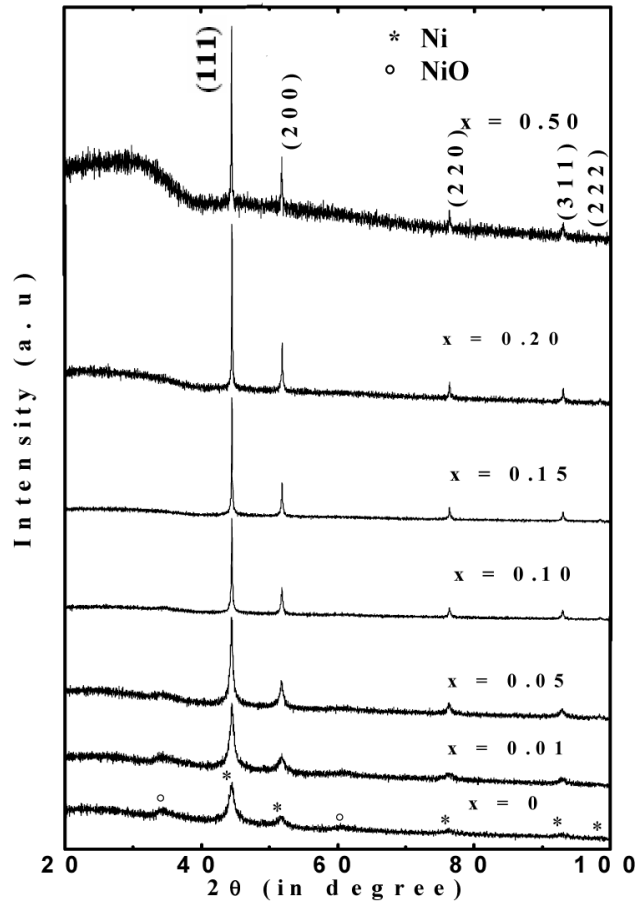
Figure 1. X-ray diffraction from Ni:xMZrO$_2$ nanostructures.

Table 1. The structural, electrical and magnetic parameters of encapsulated Ni:NiO/ZrO$_2$ nanostructures.

Sample Ni:xMZrO$_2$	Crystallite size (XRD) (nm)	Resistivity (ρ), Ω cm at 300 K	M_s (emu/g) at 300 K at 20 kOe
$x = 0$	9	3.59	13.5
$x = 0.01$	12	0.53	13.9
$x = 0.05$	21	0.14	20.5
$x = 0.10$	46	0.12	18.1
$x = 0.15$	61	2.37	16.2
$x = 0.20$	69	$\sim 10^5$	12
$x = 0.50$	72		4.2

Figure 2. XRD plots of pure SiO_2 and Fe_3O_4-coated SiO_2 particles.

disappear and the Ni crystalline peaks become stronger. The average size increases from $\sim$9 nm to 72 nm with the addition of ZrO_2 (table 1) showing clearly that it not only protects Ni from oxidation but also catalyzes the aggregation of Ni atoms into large crystallites. Figure 2 shows the amorphous nature of SiO_2 particles and single phase of Fe_3O_4 spinel structure in ferrite-coated SiO_2 samples. The XRD pattern of the Fe_3O_4, $MnFe_2O_4$ and $CoFe_2O_4$ nanoparticles correspond to the cubic ferrite, which confirms the formation of single phase for all the ferrites. The crystallite size of these ferrites was measured from XRD line broadening using Scherrer's formula, which was found to be in the range of 10–12 nm.

In figures 3–8, we show the TEM micrographs of different magnetic nanostructure systems. Figure 3 is the micrograph for iron oxide particles prepared through sonochemistry. Acicular particles with very large aspect ratio are obtained. Figures 4a and b show different shapes of Ni nanoparticles after reducing the as-prepared powder at 650°C and 750°C respectively under controlled atmosphere. A large variation in particle shape and size is observed. The average particle size varies from 30 to 150 nm for all the samples. No significant increase in particle size was observed when the temperature increases from 650°C to 750°C. The TEM micrograph and the diffraction pattern from Ni particles with NiO/ZrO_2 as shell (figure 5), show that NiO is amorphous and covers the Ni particles for $x = 0$. The diffuse ring from amorphous NiO is absent for the sample with $x = 0.1$ ZrO_2, supporting the X-ray diffraction results.
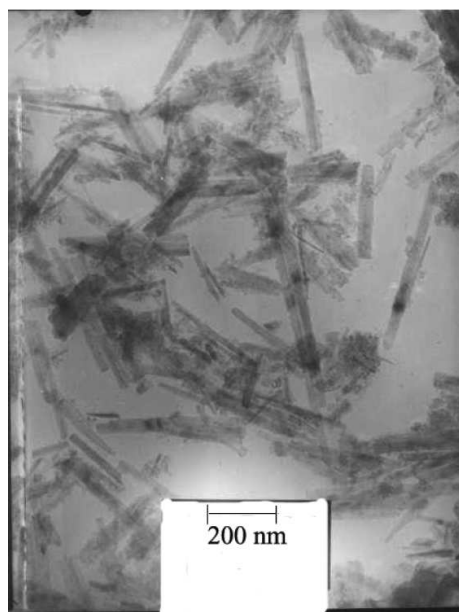
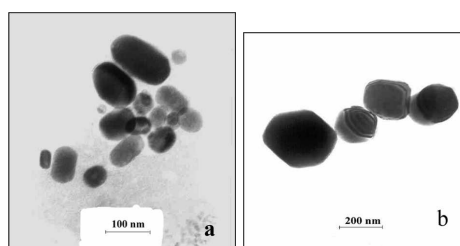**Figure 3.** TEM micrograph of acicular-shaped magnetic iron oxide particles.

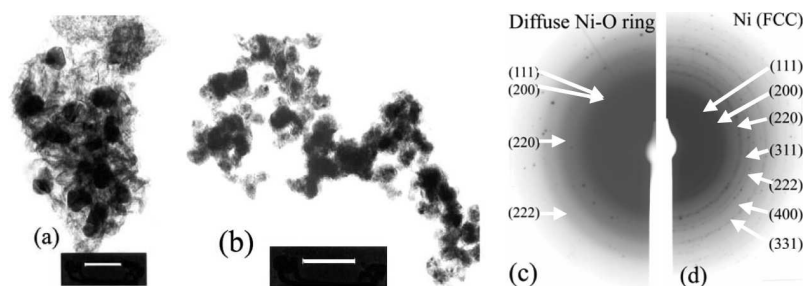**Figure 4.** TEM micrographs of different shapes of Ni nanoparticles heated at (**a**) $650°$C and (**b**) $750°$C.

Figure 5. TEM micrographs showing the presence of amorphous Ni–O encapsulate on Ni nanoparticles for sample Ni:xMZrO$_2$ nanostructures, where x corresponds to molar concentration of Zr salt in the starting solution for (**a**) $x = 0$, (**b**) $x = 0.10$. Electron diffraction pattern of (**c**) the diffused Ni–O ring and (**d**) sharp rings of Ni (fcc structure). Scale corresponds to 100 nm.

Figure 6 shows the morphology and size of the coated magnetic particle of one of the ferrofluid (Fe$_3$O$_4$). The particles are spherical in shape and well-dispersed. The physical size of the particle varies from 5 to 14 nm and mean size is about 10 nm, which is in good agreement with the crystallite size (10–12 nm).

Figure 7 shows the TEM micrograph of monodisperse SiO$_2$ spherical particles which were synthesized by modified Stober process. The silica spheres are $\sim$200 nm in diameter with a standard deviation of 3%. These spherical particles are
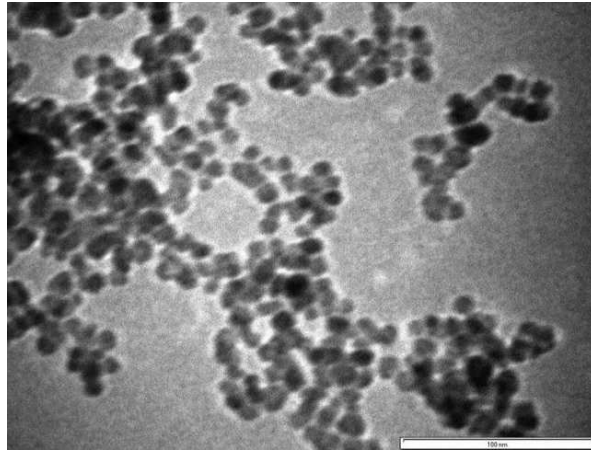
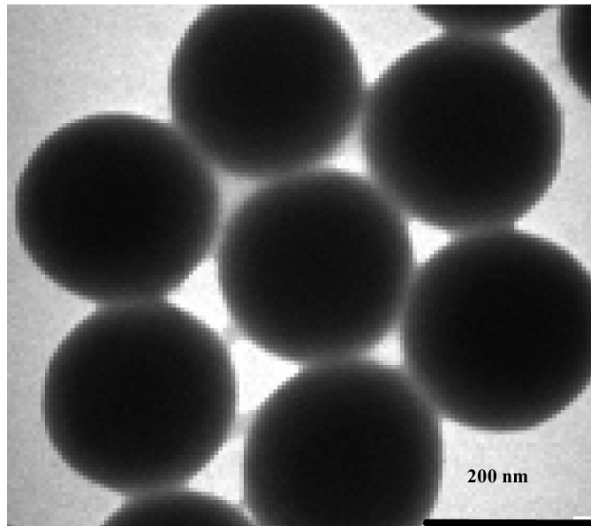**Figure 6.** TEM micrograph of coated Fe_3O_4 particle (scale: 100 nm).

Figure 7. TEM micrograph of monodisperse SiO_2 particles.

approaching hexagonal close packed arrangement in one layer, which clearly indicates the initiation of self-assembly.

Figure 8 shows the SEM micrograph of self-assembled Fe_3O_4-coated (Fe^{3+}/Fe^{2+} = 75%) SiO_2 particles. The ferrite coating is confirmed from the change in size, shape and the presence of Fe element in the particle determined from EDAX (data not shown). It is observed from SEM micrograph that there is a prominent change in average size (from $\sim$200 nm before coating to $\sim$270 nm after coating) and shape due to coating. Some bigger particles are also found in SEM image which may be attributed to agglomeration of particles.
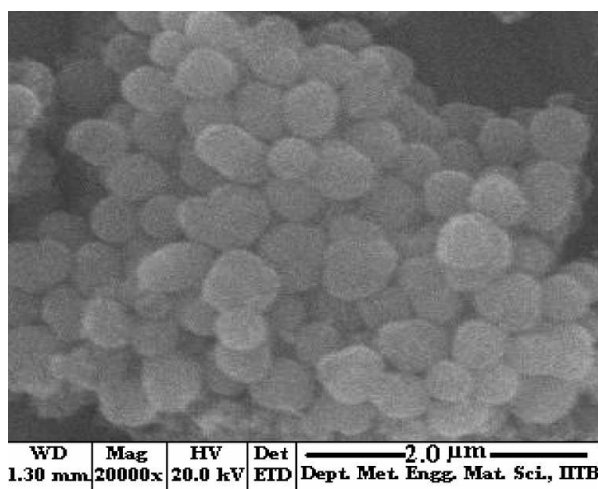
Figure 8. SEM micrograph of self-assembled Fe_3O_4-coated SiO_2 particles.

The room temperature magnetization of Ni:NiO/ZrO_2 nanostructure at a field of 20 kOe, is given in table 1 and is found to increase with the addition of ZrO_2 up to 0.05 and then decreases. The absolute value of magnetization, however, is low compared to that of pure Ni, 55 emu/g. This could be attributed to superparamagnetic nature of the particles, possible antiferromagnetic NiO layer on Ni nanoparticles and the presence of ZrO_2. It is observed that as the weight fraction of ZrO_2 increases, the crystallite size obtained from X-ray diffraction also increases. The Ni crystallites although grow with the addition of ZrO_2, become increasingly isolated leading to lack of electrical transport.

The resistivity data at room temperature for all the samples are shown in table 1. It is observed that the absolute resistivity decreases first (up to $x \leq 0.10$) and then increases with the addition of ZrO_2 ($x \geq 0.15$). These results are in agreement with the microstructural results which show that initial addition of ZrO_2 promotes Ni formation leading to a better inter-particle connectivity while it is reduced for $x \geq 0.1$ due to ZrO_2 encapsulation which is an insulator.

The typical room temperature magnetization loops of cobalt ferrite nanoparticle and Fe_3O_4-coated SiO_2 particles are depicted in figures 9a and b respectively. The results show zero coercivity, zero remanence and also nonsaturation up to 20 kOe, indicating superparamagnetic nature of ferrite particles. From figure 9b, it is observed that the specific magnetization depends on the ratio of Fe^{3+}/Fe^{2+} ions used for coating during synthesis of MPCs. The low value of saturation magnetization may be due to the presence of nonmagnetic SiO_2 core along with Fe_3O_4 shell.

Magnetic microspheres for radionuclide separation from aqueous medium were studied for the removal of europium from acidic medium. Dynamic light scattering studies indicated that majority of the magnetite polyester–polystyrene beads centered around 10 μm as shown in figure 10.

The DC magnetization data of CMPO-loaded magnetic beads are shown in figure 11. Zero coercivity and remanance confirmed that the particles were
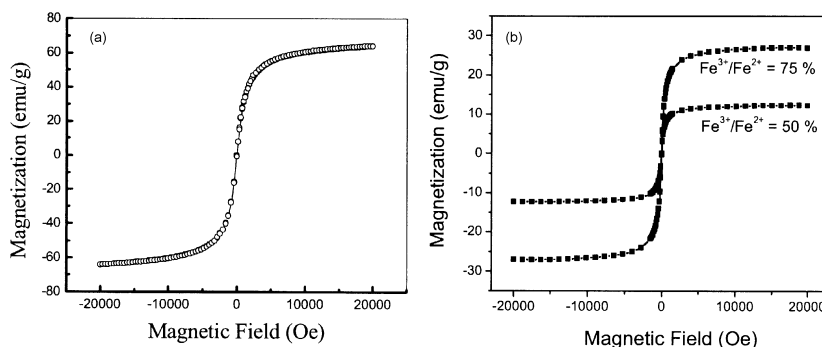
Figure 9. (**a**) Room temperature magnetization loop of coated $CoFe_2O_4$. (**b**) Specific saturation magnetization of Fe_3O_4-coated SiO_2 spheres at room temperature.
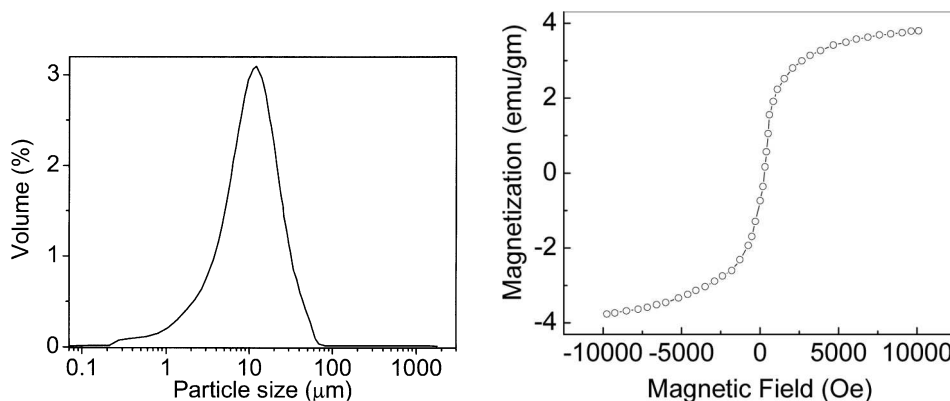

Figure 10. Particle size distribution of magnetic beads.

Figure 11. Magnetization behaviour of CMPO-loaded magnetic beads at 300 K.

superparamagnetic in nature. The magnetic filter was therefore regenerable. CMPO on magnetic beads was extracted in dodecane by ultrasonication. The common IR bands corresponding to CH bonds, the C_6H_5-P stretch (ϕ-P) and C=O stretch in pure solvent in dodecane and solvent extracted from magnetic beads are compared in figure 12.

In order to test the surface extraction behaviour of the CMPO-loaded magnetic polymer beads, magnetically assisted chemical separation was studied for the removal of europium in 2N HNO_3. Distribution coefficient, K_d, relates to the extraction capacity of the sorbent. It is expressed using the relation

$$K_d = \left(\frac{C_i - C_f}{C_f} \right) \times \frac{V}{m}, \tag{1}$$

where C_i and C_f are the initial and final radioactivity of the element in the solution before and after extraction, V is the volume of the solution and m is the mass of the solvent-loaded magnetic beads. A distribution coefficient of 1000 was obtained
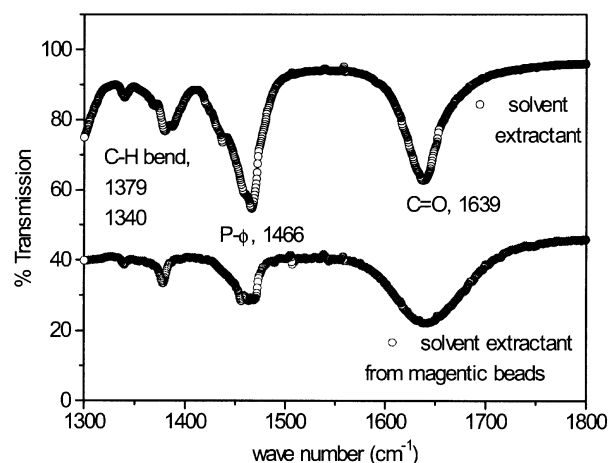
Figure 12. FTIR spectrum of solvent extracted from magnetic beads.

for the beads contacted in the presence of CMPO. In the absence of the extractant, no uptake was observed on the beads.

4.1 *Biocompatibility studies*

In vitro biological evaluation was done by SRB assay. It was found that there was dose-dependent cytotoxicity for all the magnetic fluids. It has been observed that the percentage viability of BHK 21 cells for control as well as for different magnetic fluids at 48 h of incubation is different. For Fe_3O_4 and $MnFe_2O_4$ ferrofluids, the percentage viability is more than 60% up to a concentration of 0.2 mg/ml; but less than 50% for $CoFe_2O_4$. Hence $MnFe_2O_4$ is comparable to Fe_3O_4 in terms of biocompatibility but $CoFe_2O_4$ is slightly more toxic than $MnFe_2O_4$ and Fe_3O_4. Figures 13a–d show that there is enough cell growth up to 0.2 mg/ml concentration of $MnFe_2O_4$ as compared to control whereas most of the cells die at 1.0 mg/ml concentrations. Similar trends were also observed for other magnetic fluids.

Figure 14 shows the effects of γ-Fe_2O_3 suspension of concentration 26 mg and 30 mg per ml on the viability of HeLa cells. It is observed that there is no change in cell viability of HeLa cells even after 48 h for low concentration (less than 13%). At 13% of suspension, cell viability decreased by 49% and 52% for the two suspensions and at 15% of suspensions the viability decreased by 39% and 34% respectively. The percentage viability of the cells in the present case is much higher compared to the value reported in [32].

From *in vivo* evaluation of magnetic fluid, it was found that there was no significant change in hematological parameters (data not shown) for magnetic fluids as compared to control except for the sample $CoFe_2O_4$ which exhibits a slight increase in serum glutamate pyruvic transaminase (SGPT) at its higher doses (400 mg/kg bwt). Slight increase of SGPT in $CoFe_2O_4$ might be due to mild hepatotoxic effects of $CoFe_2O_4$. This mild hepatotoxic effect of $CoFe_2O_4$ is attributed mainly to cobalt part of this ferrite as other elements are also present in Fe_3O_4 and $MnFe_2O_4$ and
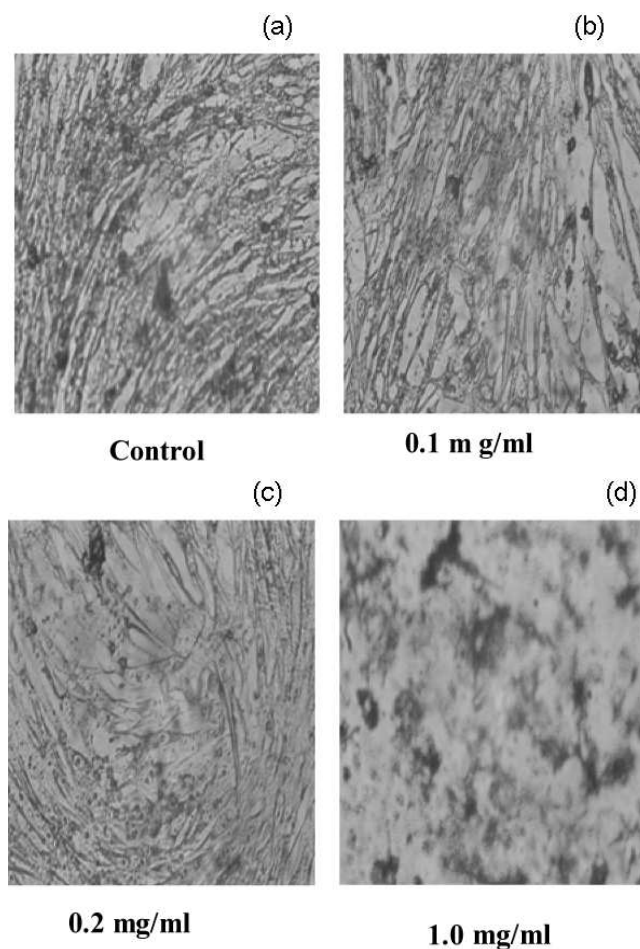
(a)   (b)

Control   0.1 m g/ml

(c)   (d)

0.2 mg/ml   1.0 mg/ml

Figure 13a–d. Micrographs of BHK21 cells (fixed with 50% trichloroacetic acid) showing cell growth for control and $MnFe_2O_4$ treated cells at 48 h of incubation (magnification $\times$ 200).

have been found to be nontoxic. Histomorphology of different organs after magnetic fluid injection for different doses of ferrite did not show any pathological alterations as compared to control indicating their biocompatibility *in vivo* up to a dose rate of 400 mg/kg body weight (bwt). Figure 15 shows that even after IV injection of 400 mg/kg bwt of $MnFe_2O_4$, there is no morphological alteration in liver. But the presence of aggregated particles and Kupffer cells is observed in liver parenchyma. Undesirable particle aggregates found in liver parenchyma could be due to dipole–dipole interaction of magnetic particles after loss of lauric acid coating. Presence of Kupffer cells implies that magnetic particles following IV administration were phagocytosed by reticulo endothelial system (RES) which is expected as no chemical modification of particle surface was done to prevent phagocytosis. However,
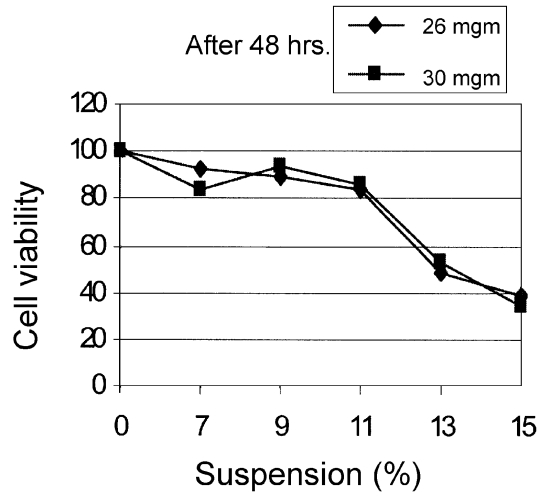
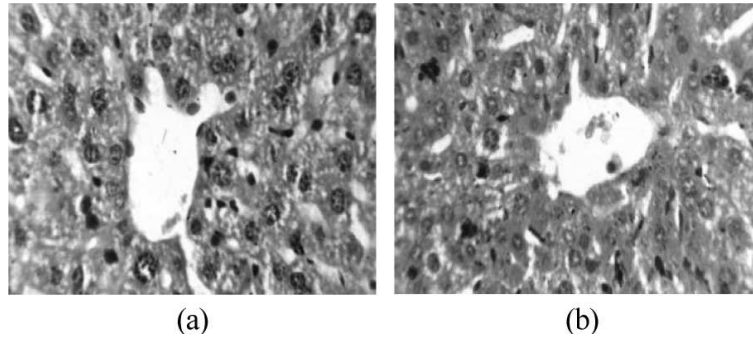**Figure 14.** Effects of 26 mg and 30 mg of γ-Fe$_2$O$_3$ per ml of suspension on the viability of HeLa cells.

Figure 15. Micrographs of mouse liver: (**a**) control and (**b**) after IV injection of MnFe$_2$O$_4$ magnetic fluid (400 mg/kg bwt) at 24 h (hematoxylene-eosin staining $\times$ 450).

instead of their presence in different organs no toxic effect has been found indicating their biocompatibility *in vivo*.

5. Conclusion

The magnetic nanostructures were synthesized by a variety of soft chemical methods including self-assembly for various applications. We have been able to achieve different shapes and sizes of nanoparticles by changing the processing conditions. Nanocomposites of Ni:NiO/ZrO$_2$s have been made successfully by a chemical reduction process using a reducing agent (NaBH$_4$). Addition of ZrO$_2$ is found to promote complete reduction of nickel nanograins and also prevent oxidation by encapsulation. Electrical transport behaviour shows better interparticle connectivity for

sample $x \leq 0.10$ while for $x \geq 0.10$ the interparticle connectivity is reduced due to ZrO_2 encapsulation. Magnetic fluids were obtained which possess all the magnetic properties for applications in hyperthermia treatment of cancer. Magnetic microspheres have been synthesized for specific applications in magnetically-assisted radioactive waste separation for removal of transuranics and other radionuclide substrates.

Acknowledgement

References

[1] D Bahadur and J Giri, *Sadhana* **28**, 639 (2003)
[2] I Willner and B Willner, *Pure Appl. Chem.* **74**, 1773 (2002)
[3] J E Sundeen and R C Buchanan, *Sens. and Actuators* **A63**, 33 (1997)
[4] V Skumryev, S Stoyanov, Y Zhang, G Hadjipanayis, D Givord and J Nogues, *Nature (London)* **423**, 850 (2003)
[5] X-C Sun and X-L Dong, *Mater. Res. Bull.* **37**, 991 (2002)
[6] J Giri, T Sriharsha and D Bahadur, *J. Mater. Chem.* **14**, 875 (2004)
[7] J Giri, S G Thakurta, J Bellare, A K Nigam and D Bahadur, *J. Magn. Magn. Mater.* **293**, 62 (2005)
[8] Q Chen, A J Rondinone, B C Chakoumakos and Z J Zhang, *J. Magn. Magn. Mater.* **194**, 1 (1999)
[9] R Vijayakumar, Y Koltypin, I Felner and A Gedanken, *Mater. Sci. Eng.* **A286**, 101 (2000)
[10] D Makovec, A Košak, A Žnidaršič and M Drofenik, *J. Magn. Magn. Mater.* **289**, 32 (2005)
[11] Y Xia, B Gates, Y Yin and Y Lu, *Adv. Mater.* **12**, 693 (2000)
[12] J D Jonnaopoulos, R D Meade and J N Winn, *Photonic crystals* (Princeton University Press, NJ, 1995)
[13] M Inoue, K I Arai, T Fujii and M Abe, *J. Appl. Phys.* **85**, 5768 (1999)
[14] A A Fedyanin, T Yoshida, K Nashimura, G Marowsky, M Inoue and O A Aktsipetrov, *J. Magn. Magn. Mater.* **258**, 96 (2003)
[15] M K Beklemishev and C M Wai, Liquid extraction, new extraction agents – crown ether extractants, in: *Separation technology in nuclear waste management* edited by T E Carleson, N Chapman and C M Wai (CRC Press, Boca Raton, FL, 1995) pp. 47–67
[16] R-S Juang, *Proc. Natl. Sci. Counc. ROC (A)* **23**, 353 (1999)
[17] L Nunez and M D Kaminski, *J. Magn. Magn. Mater.* **194**, 102 (1994)
[18] R D Ambashta, P K Wattal, S Singh and D Bahadur, *J. Magn. Magn. Mater.* **267**, 335 (2003)
[19] R D Ambashta, S M Yusuf, M D Mukadam, S Singh, P K Wattal and D Bahadur, *J. Magn. Magn. Mater.* **293**, 8 (2005)

[20] E P Horwitz and R Chiarizia, Liquid extraction, the true process – experimental studies, in: *Separation techniques in nuclear waste management* edited by T E Carleson, N Chapman and C M Wai (CRC Press, Boca Raton, FL, 1996) pp. 3–33

[21] J Giri, A Ray, S Dasgupta, D Datta and D Bahadur, *Bio-med Mater. and Eng.* **13**, 387 (2003)

[22] F Grasset, S Mornet, A Demourgues, J Portier, J Bonnet, A Vekris and E Duguet, *J. Magn. Magn. Mater.* **234**, 409 (2001)

[23] A Petri-Fink, M Chastellain, L Juillerat-Jeanneret, A Ferrari and H Hofmann, *Biomaterials* **26**, 2685 (2005)

[24] A Jordan, P Wust, R Scholz, B Tesche, H Fahling, T Mitrovics, T Vogl, J Cervos-Navarro and R Felix, *Int. J. Hyperthmia* **12**, 705 (1996)

[25] L M Lacava, V A P Garcia, S Kückelhaus, R B Azevedo, N Sadeghiani, N Buske, P C Morais and Z G M Lacava, *J. Magn. Magn. Mater.* **272**, 2434 (2004)

[26] N K Prasad, D Panda, S Singh, M D Mukadam, S M Yusuf and D Bahadur, *J. Appl. Phys.* **97**, 10Q903 (2005)

[27] J Giri, P Pradhan, T Sriharsha and D Bahadur, *J. Appl. Phys.* **97**, 10Q916 (2005)

[28] Bibhuti B Nayak, Satish Vitta, Arun K Nigam and D Bahadur, *IEEE Trans. Magn.* **41** (2005) (in press)

[29] W Stöber, A Fink and E Bohn, *J. Coll. Inter. Sci.* **26**, 62 (1968)

[30] K Nashimura, A V Baryshev, T Kodama, H Uchida and M Inoue, *J. Appl. Phys.* **95**, 6633 (2004)

[31] K Gupta, J Bishop, A Peck, J Brown, L Wilson and D Panda, *Biochemistry* **43**, 6645 (2004)

[32] A Jordan, R Scholz, P Wust, H Schirra, T Schiestel, H Schmidt and R Felix, *J. Magn. Magn. Mater.* **194**, 185 (1999)